Creating perfectly ordered quantum dot arrays via self-assembly

Feng Shi,[1] Pradeep Sharma,[1,2] and Gemunu H. Gunaratne[2]
[1]*Department of Mechanical Engineering, University of Houston, Houston, Texas 77204, USA*
[2]*Department of Physics, University of Houston, Houston, Texas 77204, USA*

(Received 18 June 2009; accepted 21 August 2009; published online 17 September 2009)

Several applications involving quantum dots require perfect long-range ordered arrays. Unfortunately, self-assembly (the choice method to fabricate quantum dots) leads to patterns that, although short range ordered, exhibit defects equivalent to grain boundaries and dislocations on a large scale. We note that rotational invariance of film growth is one reason for formation of defects, and hence study an anisotropic model of quantum dot formation. However, nonlinear stability analysis shows that even in the extreme limit of anisotropy, square arrays whose orientations are in a finite range are linearly stable; consequently structures created in the film continue to have defects. Building on insights developed by the authors earlier on a simpler monolayer self-assembly model, we propose controlling the deposition through a mask to generate ordered quantum dots arrays. General principles to estimate geometrical characteristics of the mask are given. Numerical integration of the model shows that perfectly ordered square arrays of quantum dots can indeed be created using masked deposition. © *2009 American Institute of Physics*. [DOI: 10.1063/1.3227643]

Quantum dots are nanoscale three-dimensionally confined semiconductor structures, which exhibit quantum effects such as sharp density of states. They are potentially of immense technological importance because their optical and electronic properties can be tuned using the size of a dot and the interdot distance of an array. Quantum dots are often considered as the basis for several revolutionary nanoelectronic devices and applications, e.g., next generation lighting,[1,2] lasers,[3,4] quantum computing, information storage and quantum cryptography,[5–7] biological labeling,[8] sensors,[9] and many others.[10–14] However, several applications require large arrays rather than a single quantum dot. The most promising approach to grow large-scale arrays of quantum dots is self-assembly. Unfortunately, large-scale self-assembled arrays are imperfect, consisting of multiple domains, domain walls, and defects (see Fig. 1). Since optoelectronic properties and responses acutely depend upon quantum dot size and spacing, predictable and reliable controlled applications require arrays with perfect long range order. For example, "inhomogeneous broadening" (the loss of sharp physical characteristics due to nonuniformity in the size and imperfections in long-range order) can lead to the following issues in quantum dot based lasers: spectral hole burning limits gain, broadens emission between 30 and 70 meV even for a 15% size fluctuation, hinders the "promised" temperature stabilized operation, and so on (for more information see Refs. 15–20 and references therein). Our goal in this paper is to introduce a method that can be used to generate large-scale perfectly ordered quantum dot arrays. In addition, based on nonlinear stability analysis, we provide insights into the conditions necessary for specific classes of patterns.

I. INTRODUCTION

In the present context, self-assembly is the symmetry breaking bifurcation of a homogeneous film formed by the uniform deposition of material on a substrate. It occurs as a result of competition between the wetting potential and elastic and surface energies of the film. Typically, the homogeneous solution is stable for thin films and destabilizes beyond a specific thickness. This "Stranski–Krastanow" growth has emerged as an effective and economical way to generate large-scale quantum dot arrays.[21–25] Many film materials and substrates have been identified where the scale of the quantum dots is of the order of a few nanometers.[26–29]

It is easy to understand why large-scale self-assembled arrays are seldom perfect. Consider first the case where the deposition is isotropic. When the flat film destabilizes to a self-assembled array, it loses orientational and translational symmetries. Hence there is a "Goldstone mode" of equivalent solutions, which in this case are related to each other by translations and/or rotations. In other words, an array that emerges spontaneously can have any orientation, and the specific direction along which the arrays form depends on uncontrollable factors like local stochastic effects. In a large-scale array, sites far from each other emerge with independent orientations. As these arrays grow beyond a characteristic size, they fail to merge to a single domain, thus leaving a pattern with multiply oriented domains and associated defects.

Anisotropic systems, such as the model we study in the present paper, are slightly different. Here, there is a preferred orientation for the array. However, as we show below, even in highly anisotropic systems there is a band of angles about this preferred direction for which the arrays are linearly stable. Consequently, large-scale ordered arrays do not form spontaneously and the problem of defective arrays persists.

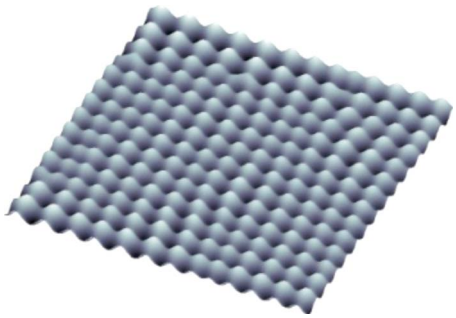

FIG. 1. (Color online) Self-assembled arrays of quantum dots in a large domain. "Defects" in the pattern are readily apparent.

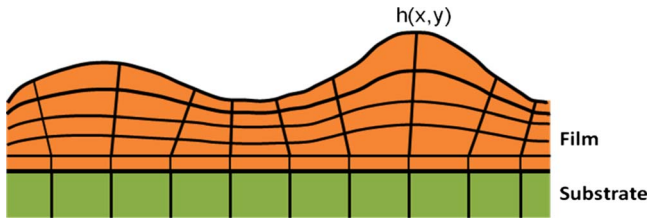

FIG. 2. (Color online) Lattice configuration of the film-substrate model.

There have been several proposals to guide the fabrication of large-scale ordered monolayer and quantum dot arrays. The use of external electric fields[30,31] was proposed to drive quantum dot formation in a predesigned arrangement. This is applicable for highly dielectric materials. The use of a lithographically prepatterned substrate as a template to guide the organization of the film (graphoepitaxy) has been proposed.[32,33] Here sites on the template are different from those outside. In Shi *et al.*,[34] we proposed regulating self-assembled monolayer formation by applying a control on the deposition using a mask. This mask is placed a finite distance above the substrate and the deposited atoms are able to diffuse to sites lying directly below the mask, thus allowing for patterns to emerge even at these locations. The broad conditions required to generate large-scale ordered monolayer arrays were identified.[34]

The aim of the work reported here is to demonstrate that the formation of three dimensional quantum dot arrays can also be controlled, by suitable masking of the deposition, to the point that perfect order may be achieved. In Sec. II, we discuss energy components that determine the shape of the film and outline a particular phenomenological model that was introduced previously by other researchers. The results reported here relate to the formation of square arrays of quantum dots. In Sec. III, we determine conditions for their spontaneous formation. The nonlinear stability analysis required to evaluate the stability maps for square arrays is given in the Appendix. We find that even in highly anisotropic systems, there is a range of orientations where square arrays are linearly stable. Consequently, it is not possible to obtain large-scale ordered square arrays without some form of external guidance. In Sec. IV, we conduct numerical integrations of the model to show that typical patterns generated in the system are indeed defective, and that suitable masking of the deposit can be used to create large-scale defect-free ordered arrays. Section V provides a discussion of our results and some caveats.

II. THE MODEL SYSTEM

The phenomenological model adopted in this paper was introduced and analyzed in Ref. 22. We summarize some conclusions in this section. A solid substrate occupies the semi-infinite region $z<0$ (with normal [001]), and a film of different material is slowly deposited epitaxially or through chemical vapor deposition. The film shape is characterized by the height $h(x,y)$ of the film, which is assumed to fill the region $0<z<h(x,y)$. The substrate is assumed to remain unchanged by the deposition and the strain on the film is assumed to be small enough so that strain-induced renormalization of the material properties can be ignored. Hence, the energy of the system consists of three components.

(1) Wetting interaction between the substrate and the film, which is typically appreciable only close to the interface. The expression used in Ref. 22 is

$$w = -w_0\left(\frac{h}{\delta}\right)^{-\alpha}\exp\left(-\frac{h}{\delta}\right). \tag{1}$$

Here w_0 represents the intensity of the wetting potential, δ is the characteristic wetting length, and α shows the singularity of the wetting potential as $h\to 0$. Note that the wetting potential favors a flat film.

(2) When lattice sizes of the substrate and the film are close, atoms of the film tend to align with those of the substrate.[35,36] The stress caused by alignment increases with the thickness of the film and can be released by wrinkling.

(3) The free surface energy of the film. Isotropic surface energy favors a smaller surface area, and hence a flat film. However, if the surface energy γ is anisotropic, it can destabilize the homogeneous film. For films with cubic crystal symmetry, it can be shown that[22,23]

$$\gamma = -\lambda(\partial_x h, \partial_y h)\kappa + \tfrac{1}{2}v\Delta^2 h, \tag{2}$$

where $\lambda(\partial_x h, \partial_y h)$ is the anisotropic surface energy density associated with local surface slopes and the crystal properties of the thin film and κ is the curvature of the free surface in the reference configuration (Fig. 2). When λ is isotropic, κ can be obtained in the current configuration as

$$\kappa = \frac{\partial_x^2 h[1+(\partial_y h)^2] - 2\partial_x h\partial_y h\partial_{xy} h + \partial_y^2 h[1+(\partial_x h)^2]}{[1+(\partial_x h)^2+(\partial_y h)^2]^{3/2}}. \tag{3}$$

The second term of Eq. (2), $1/2v(\Delta h)^2$, is the additional energy needed to account for the corners of the quantum dots (if present).

When the surface energy is isotropic, wetting potential and surface energy effects stabilize the homogeneous film, while elastic energy destabilizes it. The typical structures observed following the instability in symmetric systems are hexagonal arrays. In this paper, we wish to analyze self-assembled *square* arrays—an important pattern style from a technological standpoint. This requires the system to be an-

isotropic and, following Ref. 22, we incorporate the anisotropy in the surface energy in our work. An additional implication of this choice is that surface energy can then destabilize the homogeneous film. In Ref. 22 the elastic energy terms are neglected for simplicity, even though they will be needed for quantitative comparison. We emphasize here that the novel contributions of the present work are not related to the creation of the self-assembly model but rather a thought process to take a pre-existing self-assembly model and "force" it to create defect-free patterns. Our methodology could very well be implemented (at the cost of additional complexity) with inclusion of elastic energy and possibly other refinements. With this caveat and these approximations, the total chemical potential of the system is

$$\mu = \gamma + w. \tag{4}$$

Changes in the film shape are assumed to occur through mass transport on the surface of the thin film. Near the onset of instability of the homogeneous film, the derivatives of $h(x,y)$ are expected to be small. Under these conditions, the spatiotemporal dynamics of $h(x,y)$ reduces to[37]

$$\partial_t h = \frac{DS\Omega}{RT}\Delta_s[\sigma\Delta h + v\Delta^2 h - a(\partial_x h)^2\partial_x^2 h - b(\partial_y h)^2\partial_x^2 h - b(\partial_x h)^2\partial_y^2 h - a(\partial_y h)^2\partial_y^2 h + 4b\partial_x h\partial_y h\partial_x\partial_y h + w], \tag{5}$$

where D is the surface atom diffusivity (cm^2/s), R is the Boltzmann constant (J/K), T is absolute temperature (K), and Ω is the molecular volume. a and b are parameters that quantify the anisotropy of the surface energy.

Rescaling in-plane distances by $l_1=(v/\sigma)^{1/2}$, the normal distances by $l_2=(v/a)^{1/2}$, and the time scale by $\tau = v^2/(DS\Omega/RT)\sigma^3$, the equation is reduced to

$$\partial_t h = \Delta_s[\Delta h + \Delta^2 h - (\partial_x h)^2\partial_x^2 h - q(\partial_y h)^2\partial_x^2 h - q(\partial_x h)^2\partial_y^2 h - (\partial_y h)^2\partial_y^2 h + 4q\partial_x h\partial_y h\partial_x\partial_y h + W] \tag{6}$$

where $q=b/a$ and $W=[a^{(\alpha+1)/2}/\sigma^2 v^{(\alpha-1)/2}]w$. Equation (6) is the model used in our studies. In Sec. III, we outline the linear stability analysis to study the destabilization of the homogenous film. The nonlinear stability analysis to evaluate stability domains for striped and square arrays is given in the Appendix.

III. STABILITY ANALYSIS FOR SQUARE ARRAYS

Before conducting the stability analysis, we emphasize that our primary aim is to study square quantum dot arrays, which are known to stabilize when the surface energy anisotropy is sufficiently high.[22] Accordingly, we analyze the extreme limit of anisotropy when q is zero. Our aim in this section is to show that even when the anisotropy is extreme, the orientation of linearly stable square arrays in not unique. We make the simplification that the deviation of the free surface of the thin film away from the flat surface is negligible during the quantum dot formation, and thus approximate the surface Laplacian in Eq. (6) by the planar Laplacian. The corrections due to this approximation are of a higher order than terms considered here.

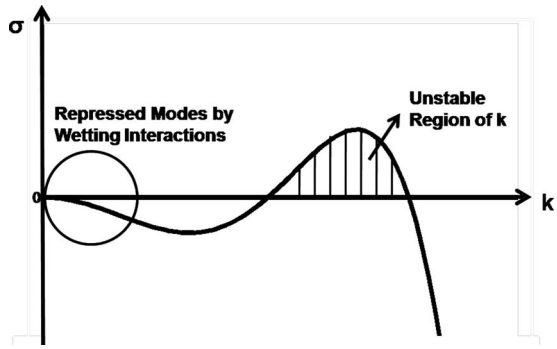

FIG. 3. The linear dispersion curve. The conservation of material is reflected in the vanishing of σ at $k=0$.

Expanding the homogeneous film thickness as $h(x,y) = h_0 + \tilde{h}e^{i(k_x x + k_y y)}e^{\sigma t}$ and expanding to linear order[22] gives the linear dispersion relation (see Fig. 3)

$$\sigma = -k^2\left[\left(k^2 - \tfrac{1}{2}\right)^2 + r\right]. \tag{7}$$

Here σ is the linear growth rate of the perturbation ($\sim e^{i\mathbf{k}\cdot\mathbf{x}}$) of a planar film with initial thickness h_0, k denotes the magnitude of the wave vector in the reciprocal space, and $r = (\partial W/\partial h)_{h=h_0} - \frac{1}{4}$ is the bifurcation parameter.

From Eq. (7), the critical wave number, where the (linear) growth away from the homogeneous film is fastest, is found to be $k_c=(2+\sqrt{1+12r/6})^{1/2}$. The next step is to identify the stability map for square arrays. We use a symmetric (in x and y) formulation of the traditional multiple scale analysis for this purpose.[38,39] The analysis is outlined in the Appendix. We find that even when the anisotropy is extreme, there is no unique orientation for stable square arrays. In fact, there is a finite range of angles where they are linearly stable. Consequently, typical large-scale arrays can be expected to contain domain walls and defects.

As an example, we consider the deposition of germanium on a silicon [001] substrate (Fig. 4). The relevant control parameters for this case are $a=11.1$ J/m^2, $w=8.2\times10^5$ J/m^3, $\sigma=0.2$ J/m^2, $v=5.0\times10^{-19}$ J, and $\alpha=3$.[22] The thickness of the film was chosen to be 3.82 nm. Under these conditions, nonlinear stability analysis shows that square arrays are stable when $\theta<27.5°$. The striped arrays are un-

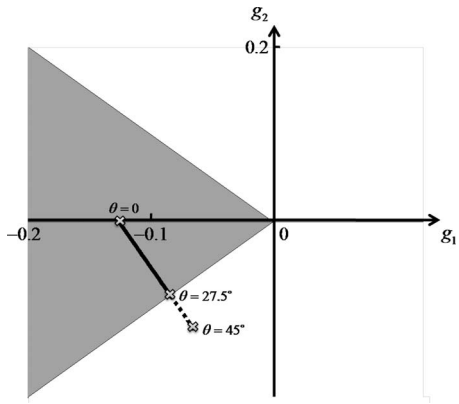

FIG. 4. Stability boundaries of square patterns for control parameters appropriate for the slow deposition of germanium on a silicon [001] substrate.

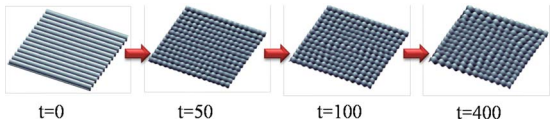

FIG. 5. (Color online) The transition from an unstable stripe pattern to the square array of quantum dots.

stable here. The entire process of the destabilization of a striped pattern to a square array is demonstrated by an integration of Eq. (6) in a domain of size 24×24 nm^2 shown in Fig. 5.

Note that if a suitable model system for a specific experimental setup is not available, parameter ranges where square arrays are stable need to be determined experimentally.

IV. LARGE-SCALE DEFECT-FREE QUANTUM DOT ARRAYS

Although self-assembly can be an inexpensive way to create quantum dot arrays, as alluded to earlier, self-assembled arrays are irregular. In a previous study, we proposed that large-scale ordered monolayer patterns can be created by a suitable masking of the deposition.[34] There, it was also shown that geometrical properties of the mask can be deduced by studying the spatial-temporal dynamics of monolayer growth. In this section, we wish to demonstrate that the same technique can be used as a control to create perfectly ordered *three* dimensional quantum dot arrays as well.

The integration of the model system (6) was conducted using the pseudospectral method. It provides a highly efficient implementation and boosts the computational speed. In Fourier space, Eq. (6) can be expressed as

$$\frac{\partial H}{\partial t} = k^2 H - k^6 H + k^2 N, \tag{8}$$

in which $H=H(k)$ is the Fourier transform of $h(x,y)$ [i.e., $H(k)=\Sigma h(x,y)e^{i\mathbf{k}\cdot\mathbf{x}}$], k is the magnitude of $\mathbf{k}$, and $N(k)$ denotes the Fourier transform of the nonlinear terms in Eq. (6).

Equation (8) was integrated using a semi-implicit scheme, where linear terms are calculated exactly, and the nonlinear terms implicitly to ensure numerical stability without loss of accuracy. Then, Eq. (8) is simplified to

$$H^{t+1} = \frac{H^t + k^2 N^t \Delta t}{1 - k^4 \Delta t + k^6 \Delta t}, \tag{9}$$

where the superscripts indicate the time and Δt is the time step that is set to 0.001 for our simulation. We use periodic boundary conditions and a domain of size 971×971 nm^2. Each side of the domain is partitioned into 1024 lattice points.

We have chosen a highly anisotropic model ($q=0$), and the square arrays are mostly aligned in the x and y directions. However, as discussed before all square arrays oriented by an angle less than 27.5° from it are also linearly stable for our film, whose thickness is 3.82 nm. As a result of the competition between these arrays, large aspect ratio systems contain multiple domains, grain boundaries, and defects, see Fig. 6(a).

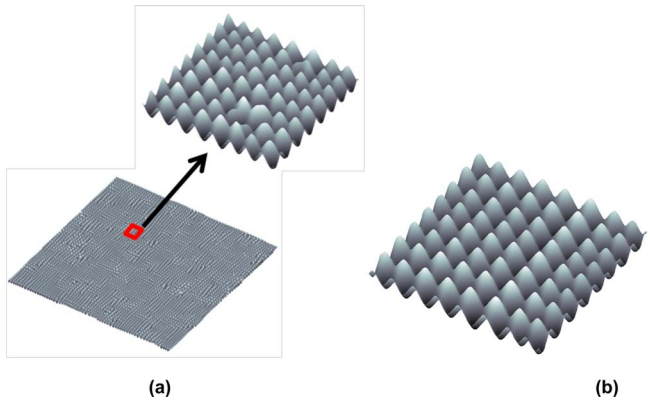

FIG. 6. (Color online) Square arrays obtained from the numerical integration of Eq. (6). The pattern is generated with the material parameters $a=11.1$ J/m^2, $w=8.2\times10^5$ J/m^3, $\sigma=0.2$ J/m^2, $v=5.0\times10^{-19}$ J, and $\alpha=3$. (a) The domain of size 971×971 nm^2 units with periodic boundary conditions. (b) The domain of size 121×121 nm^2 units with periodic boundary conditions.

On the other hand, in a sufficiently small region (specifically, one smaller than the characteristic domain size), self-assembled arrays are ordered. Figure 6(b) shows such a pattern formed in a domain with periodic boundary conditions. The creation of perfect quantum dot arrays for this domain is repeatable. Can this observation be exploited to prevent defect formation in large-scale arrays? For monolayer self-assembly, we proposed the use of a mask to control the deposition in order to partition a large area into smaller subregions in which ordered self-assembled arrays could form. We next demonstrate that the same algorithm applies to quantum dot formation as well.

Figure 7(a) shows the setup with the mask placed a finite distance above the substrate. (Note that we have assumed that the deposition occurs normal to the substrate, and hence our results are independent of the distance between the mask and the substrate.) Since the self-assembled array has square symmetry the mask is required to have this symmetry as

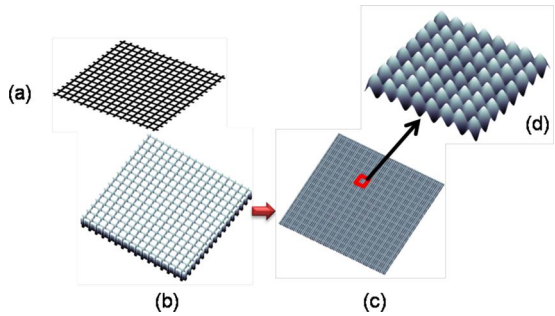

FIG. 7. (Color online) An ordered square array generated when the deposition is controlled with a suitable mask shown in (a). (b) The shape of the film immediately after the deposition. (c) The quantum dot array that results from self-assembly. (d) The arrays is perfectly ordered as can be seen from an expanded view. Note that as each subregion in (a) begins to destabilize, the self-assembled arrays form with their symmetry axes parallel to the directions of the mask.

well.[34] Geometrical characteristics of the mask can be deduced by the following considerations. The width of the stripes of the mask is required to be smaller than the diffusion length of the deposit on the substrate, since we need atoms to be able to move to all sites below the mask. On the other hand, openings of the mask need to be smaller than the characteristic domain size of the quantum dot array.[34] Interestingly, both these quantities can be obtained purely experimentally by an analysis of the spatiotemporal dynamics of self-assembly in a large domain.[34] Specifically, it is known that the structure factor $S(t)$ relaxes in two stages. During the first, domain-forming stage $S(t) \sim t^{-1/2}$. A slower, domain-coarsening stage follows. The diffusion length of the atoms deposited on the substrate is the inverse of $S(t)$ at the end of the domain forming stage, while the characteristic domain size is the inverse of the long-time value of $S(t)$.[34]

For our control parameters, the width of the stripes of the mask is ~20 nm and the distance between stripes is ~42 nm. Such masks can be manufactured with current technology[40] using very elaborate methods. However, note that the mask can be used repeatedly. The mask itself is not perfect. Current etching techniques introduce a 5%–10% level of stochasticity in the width of a stripe where width is ~20 nm.[40] In our integration (Fig. 7) we have used masks with this level of irregularity. *Imperfections* in the mask do not preclude the formation of perfect quantum dot arrays.

Following the stability analysis of Sec. III and the Appendix, we use an initial thickness of the germanium film of ~3.82 nm with a small amount of random noise. Initially, there is no deposit at locations below the mask. Figure 7(b) shows the initial deposit of the film on the Si substrate. The system is integrated from these initial conditions. The film in each region self-assembles independently. However, in each domain the orientation defined by the mask provides a (weak) guide to the square array; in fact, the two symmetry axes of the self-assembled square array lie parallel to the directions of the mask. Furthermore, diffusion of the film material allows for the quantum dot array to extend to sites below the mask. Consequently, as seen from Figs. 7(c) and 7(d) the final self-assembled array is ordered on the large scale.

V. CONCLUSIONS AND DISCUSSION

The question we address in this paper is whether a general scheme can be devised to prevent the formation of defects in self-assembled arrays of quantum dots. We studied a highly anisotropic model system where defects are least likely to form. However, we find that even in this case, square arrays with multiple orientations can be linearly stable, thus setting the stage for the spontaneous generation of defective structures. Indeed, as seen in Fig. 6, square arrays formed under these conditions are imperfect.

We note, however, that self-assembly can give ordered arrays in sufficiently small regions presumably due to the slight bias provided by the boundary conditions. Our proposal, based on this observation, was to partition the domain into smaller segments by selective masking of the deposit. Interestingly, geometrical properties of the mask can be deduced by analyzing the dynamics of the structure factor in an experimental realization of self-assembly in the system.

We hope our work motivates an experimental study of the proposed algorithm to create large-scale ordered quantum dot arrays. As we outlined for the deposition of germanium on a Si [001] substrate, masks at the required size can be manufactured using current technology. The level of errors incurred in the manufacturing process does not preclude the self-assembly of large-scale ordered arrays.

ACKNOWLEDGMENTS

The research was partially funded by ONR Young Investigator Award (P.S. and F.S.), NSF (Grant No. CMMI-0709293) (G.H.G.), and grants from the Texas Higher Education Coordination Board and the Texas Center for Superconductivity (G.H.G.).

APPENDIX: MULTIPLE-SCALE EXPANSION OF THE NONLINEAR TERMS IN THE EVOLUTION EQUATION

The starting point of nonlinear stability analysis is to note that the destabilization of the homogeneous film leads to local arrays (striped, square, and hexagonal) that vary over a scale much larger than the characteristic scale of the array. A systematic expansion is implemented by writing variations on the large scale by rescaling spatial variables x and y by a factor ε.[41] Specifically,

$$X = \varepsilon x, \quad Y = \varepsilon y. \tag{A1}$$

Linear expansion of the spatiotemporal dynamics near the onset reveals that the temporal variable t and the bifurcation parameter contribute at the order of ε^2. Thus, the appropriate scalings are

$$T = \varepsilon^2 t, \quad r = \varepsilon^2 r_2. \tag{A2}$$

Thus, derivatives of the film thickness are expanded as

$$\partial_x = \partial_x + \varepsilon \partial_X, \quad \partial_y = \partial_y + \varepsilon \partial_Y, \quad \partial_t = \varepsilon^2 \partial_T, \tag{A3}$$

where ∂_x, ∂_y act only on the "fast" variables (i.e., on the scale of the basic array) and ∂_X, ∂_Y act only on the "slow" variables (i.e., changes in the arrays). Following this separation the slow and fast variables are viewed as independent.

The operators in Eq. (6) can be divided into linear and nonlinear components $L(h)$ and $N(h)$. $L(h)$ can be expanded in powers of ε as

$$L = L_0 + \varepsilon L_1 + \varepsilon^2 L_2 + \varepsilon^3 L_3 + \text{h.o.t.}, \tag{A4}$$

where

$$L_0 = (\partial_x^2 + \partial_y^2)^2 (1 + \partial_x^2 + \partial_y^2),$$

$$L_1 = 2(\partial_X \partial_x + \partial_Y \partial_y)[2(\partial_x^2 + \partial_y^2) + 3(\partial_x^2 + \partial_y^2)^2],$$

$$L_2 = (\partial_X^2 + \partial_Y^2)(\partial_x^2 + \partial_y^2)[2 + 3(\partial_x^2 + \partial_y^2)] + 4(\partial_X \partial_x + \partial_Y \partial_y)^2 [1 + 3(\partial_x^2 + \partial_y^2)],$$

$$L_3 = 4(\partial_X\partial_x + \partial_Y\partial_y)[5(\partial_X\partial_x + \partial_Y\partial_y)^2 + 3(\partial_X\partial_x - \partial_Y\partial_y)^2 + \partial_x^2 + \partial_y^2],$$

and h.o.t. denotes higher order terms.

The thickness of the thin film $h(x,y)$ is expanded as

$$h = h_0 + \varepsilon h_1 + \varepsilon^2 h_2 + \varepsilon^3 h_3 + \varepsilon^4 h_4 + \text{h.o.t.} \tag{A5}$$

Next, expanding Eq. (6) by substituting Eqs. (A3)–(A5) we find that

$$\begin{aligned} L(h) &\to (L_0 + \varepsilon L_1 + \varepsilon^2 L_2 + \varepsilon^3 L_3) \\ &\quad \times (h_0 + \varepsilon h_1 + \varepsilon^2 h_2 + \varepsilon^3 h_3 + \varepsilon^4 h_4) \\ &= \varepsilon L_0 h_1 + \varepsilon^2 (L_0 h_2 + L_1 h_1) + \varepsilon^3 (L_0 h_3 + L_1 h_2 + L_2 h_1) \\ &\quad + \varepsilon^4 (L_0 h_4 + L_1 h_3 + L_2 h_2 + L_3 h_1). \end{aligned} \tag{A6}$$

The corresponding expansion of $N(h)$ in the small-slope approximation is derived as follows:

$$\begin{aligned} N(h) = \Delta[&-(\partial_x h)^2 \partial_x^2 h - q(\partial_y h)^2 \partial_x^2 h - q(\partial_x h)^2 \partial_y^2 h \\ &- (\partial_y h)^2 \partial_y^2 h + 4q\partial_x h \partial_y h \partial_x \partial_y h + W]. \end{aligned} \tag{A7}$$

The first term in $N(h)$ becomes

$$\begin{aligned} \Delta[(\partial_x h)^2 \partial_x^2 h] &\to [(\partial_x + \varepsilon\partial_X)^2 + (\partial_y + \varepsilon\partial_Y)^2][((\partial_x + \varepsilon\partial_X)(\varepsilon h_1 + \varepsilon^2 h_2 + \varepsilon^3 h_3 + \varepsilon^4 h_4))^2 (\partial_x + \varepsilon\partial_X)^2 (\varepsilon h_1 + \varepsilon^2 h_2 + \varepsilon^3 h_3 + \varepsilon^4 h_4)] \\ &= \varepsilon^3 (\partial_x^2 + \partial_y^2)[(\partial_x h_1)^2 \partial_x^2 h_1] + \varepsilon^4 [(\partial_x^2 + \partial_y^2)((\partial_x h_1)^2 (\partial_x^2 h_2)) + 2(\partial_x^2 + \partial_y^2)((\partial_x h_1)^2 \partial_x \partial_X h_1) + 2(\partial_x^2 + \partial_y^2)(\partial_x h_1 \partial_x h_2 \partial_x^2 h_1) \\ &\quad + 2(\partial_x^2 + \partial_y^2)(\partial_x h_1 \partial_X h_2 \partial_x^2 h_1) + 2(\partial_X \partial_x + \partial_Y \partial_y)((\partial_x h_1)^2 \partial_x^2 h_1)] + \text{h.o.t.} \end{aligned} \tag{A8}$$

The other terms in $N(h)$ can be derived in the similar manner,

$$\begin{aligned} q\Delta[(\partial_y h)^2 \partial_x^2 h] &\to q[(\partial_x + \varepsilon\partial_X)^2 + (\partial_y + \varepsilon\partial_Y)^2][((\partial_y + \varepsilon\partial_Y)(\varepsilon h_1 + \varepsilon^2 h_2 + \varepsilon^3 h_3 + \varepsilon^4 h_4))^2 (\partial_x + \varepsilon\partial_X)^2 (\varepsilon h_1 + \varepsilon^2 h_2 + \varepsilon^3 h_3 + \varepsilon^4 h_4)] \\ &= q\varepsilon^3 (\partial_x^2 + \partial_y^2)[(\partial_y h_1)^2 \partial_x^2 h_1] + q\varepsilon^4 [(\partial_x^2 + \partial_y^2)((\partial_y h_1)^2 (\partial_x^2 h_2)) + 2(\partial_x^2 + \partial_y^2)((\partial_y h_1)^2 \partial_x \partial_X h_1) \\ &\quad + 2(\partial_x^2 + \partial_y^2)(\partial_y h_1 \partial_y h_2 \partial_x^2 h_1) + 2(\partial_x^2 + \partial_y^2)(\partial_y h_1 \partial_Y h_2 \partial_x^2 h_1) + 2(\partial_X \partial_x + \partial_Y \partial_y)((\partial_y h_1)^2 \partial_x^2 h_1)] + \text{h.o.t.}, \end{aligned} \tag{A9}$$

$$\begin{aligned} \Delta[(\partial_y h)^2 \partial_y^2 h] &\to [(\partial_x + \varepsilon\partial_X)^2 + (\partial_y + \varepsilon\partial_Y)^2][((\partial_y + \varepsilon\partial_Y)(\varepsilon h_1 + \varepsilon^2 h_2 + \varepsilon^3 h_3 + \varepsilon^4 h_4))^2 (\partial_y + \varepsilon\partial_Y)^2 (\varepsilon h_1 + \varepsilon^2 h_2 + \varepsilon^3 h_3 + \varepsilon^4 h_4)] \\ &= \varepsilon^3 (\partial_x^2 + \partial_y^2)[(\partial_y h_1)^2 \partial_y^2 h_1] + \varepsilon^4 [(\partial_x^2 + \partial_y^2)((\partial_y h_1)^2 (\partial_y^2 h_2)) + 2(\partial_x^2 + \partial_y^2)((\partial_y h_1)^2 \partial_y \partial_Y h_1) + 2(\partial_x^2 + \partial_y^2)(\partial_y h_1 \partial_y h_2 \partial_y^2 h_1) \\ &\quad + 2(\partial_x^2 + \partial_y^2)(\partial_y h_1 \partial_Y h_2 \partial_y^2 h_1) + 2(\partial_X \partial_x + \partial_Y \partial_y)((\partial_y h_1)^2 \partial_y^2 h_1)] + \text{h.o.t.}, \end{aligned} \tag{A10}$$

$$\begin{aligned} q\Delta[(\partial_x h)^2 \partial_y^2 h] &\to q[(\partial_x + \varepsilon\partial_X)^2 + (\partial_y + \varepsilon\partial_Y)^2][((\partial_x + \varepsilon\partial_X)(\varepsilon h_1 + \varepsilon^2 h_2 + \varepsilon^3 h_3 + \varepsilon^4 h_4))^2 (\partial_y + \varepsilon\partial_Y)^2 (\varepsilon h_1 + \varepsilon^2 h_2 + \varepsilon^3 h_3 + \varepsilon^4 h_4)] \\ &= q\varepsilon^3 (\partial_x^2 + \partial_y^2)[(\partial_x h_1)^2 \partial_y^2 h_1] + q\varepsilon^4 [(\partial_x^2 + \partial_y^2)((\partial_x h_1)^2 (\partial_y^2 h_2)) + 2(\partial_x^2 + \partial_y^2)((\partial_x h_1)^2 \partial_y \partial_Y h_1) \\ &\quad + 2(\partial_x^2 + \partial_y^2)(\partial_x h_1 \partial_x h_2 \partial_y^2 h_1) + 2(\partial_x^2 + \partial_y^2)(\partial_x h_1 \partial_X h_2 \partial_y^2 h_1) + 2(\partial_X \partial_x + \partial_Y \partial_y)((\partial_x h_1)^2 \partial_y^2 h_1)] + \text{h.o.t.}, \end{aligned} \tag{A11}$$

$$\begin{aligned} 4q\Delta(\partial_x h \partial_y h \partial_x \partial_y h) &\to 4q[(\partial_x + \varepsilon\partial_X)^2 + (\partial_y + \varepsilon\partial_Y)^2][((\partial_x + \varepsilon\partial_X)(\varepsilon h_1 + \varepsilon^2 h_2 + \varepsilon^3 h_3 + \varepsilon^4 h_4)) \\ &\quad \times ((\partial_y + \varepsilon\partial_Y)(\varepsilon h_1 + \varepsilon^2 h_2 + \varepsilon^3 h_3 + \varepsilon^4 h_4))(\partial_x + \varepsilon\partial_X)(\partial_y + \varepsilon\partial_Y)(\varepsilon h_1 + \varepsilon^2 h_2 + \varepsilon^3 h_3 + \varepsilon^4 h_4)] \\ &= 4q\varepsilon^3 (\partial_x^2 + \partial_y^2)[\partial_x h_1 \partial_y h_1 \partial_x \partial_y h_1] + 4q\varepsilon^4 [(\partial_x^2 + \partial_y^2)(\partial_x h_1 \partial_y h_1 \partial_x \partial_y h_2) + (\partial_x^2 + \partial_y^2)(\partial_x h_1 \partial_y h_1 \partial_x \partial_Y h_2) \\ &\quad + (\partial_x^2 + \partial_y^2)(\partial_x h_1 \partial_y h_1 \partial_X \partial_y h_2) + (\partial_x^2 + \partial_y^2)(\partial_x h_1 \partial_y h_2 \partial_x \partial_y h_1) + (\partial_x^2 + \partial_y^2)(\partial_x h_2 \partial_y h_1 \partial_x \partial_y h_1) \\ &\quad + (\partial_x^2 + \partial_y^2)(\partial_x h_1 \partial_Y h_1 \partial_x \partial_y h_1) + (\partial_x^2 + \partial_y^2)(\partial_X h_1 \partial_y h_1 \partial_x \partial_y h_1) + 2(\partial_X \partial_x + \partial_Y \partial_y)(\partial_x h_1 \partial_y h_1 \partial_x \partial_y h_1)] + \text{h.o.t.} \end{aligned} \tag{A12}$$

For the wetting potential, we need to perform Taylor expansion on W, which leads to

$$\begin{aligned} \Delta W &= [(\partial_x + \varepsilon\partial_X)^2 + (\partial_y + \varepsilon\partial_Y)^2](w_0 + w_1\delta h + w_2\delta h^2 + w_3\delta h^3) \\ &= \varepsilon\left[\tfrac{1}{4}(\partial_x^2 + \partial_y^2)h_1\right] + \varepsilon^2\left[\tfrac{1}{4}(\partial_x^2 + \partial_y^2)h_2 + \tfrac{1}{2}(\partial_X\partial_x + \partial_Y\partial_y)h_1 + w_2(\partial_x^2 + \partial_y^2)h_1^2\right] + \varepsilon^3\left[\tfrac{1}{4}(\partial_x^2 + \partial_y^2)h_3 - r_2(\partial_x^2 + \partial_y^2)h_1\right. \\ &\quad \left. + 2w_2(\partial_x^2 + \partial_y^2)(h_1h_2) + w_3(\partial_x^2 + \partial_y^2)h_1^3\tfrac{1}{2}(\partial_X\partial_x + \partial_Y\partial_y)h_2 + 2w_2(\partial_X\partial_x + \partial_Y\partial_y)h_1^2 + \tfrac{1}{4}(\partial_X^2 + \partial_Y^2)h_1\right] \\ &\quad + \varepsilon^4\left[\tfrac{1}{2}(\partial_X\partial_x + \partial_Y\partial_y)h_3 + \tfrac{1}{4}(\partial_x^2 + \partial_y^2)h_4 - r_2(\partial_x^2 + \partial_y^2)h_2 + 2w_2(\partial_x^2 + \partial_y^2)(h_1h_3) + w_2(\partial_x^2 + \partial_y^2)h_2^2 + 3w_3(\partial_x^2 + \partial_y^2)(h_1^2h_2)\right. \\ &\quad \left. - 2r_2(\partial_X\partial_x + \partial_Y\partial_y)h_1 + 4w_2(\partial_X\partial_x + \partial_Y\partial_y)h_1h_2 + 2w_3(\partial_X\partial_x + \partial_Y\partial_y)h_1^3 + \tfrac{1}{4}(\partial_X^2 + \partial_Y^2)h_2 + w_2(\partial_X^2 + \partial_Y^2)h_1^2\right], \end{aligned} \tag{A13}$$

where $\delta h = h - h_0 = \varepsilon h_1 + \varepsilon^2 h_2 + \varepsilon^3 h_3 + \varepsilon^4 h_4 + \text{h.o.t.}$ w_0, w_1, and w_2 are the coefficients of the Taylor expansion of W from the lowest order to the third order,

$$w_1 = \frac{1}{4} - r_2\varepsilon^2 = \frac{\partial}{\partial h}\left[-w\left(\frac{h}{\delta}\right)^{-\alpha_w} e^{-h/\delta}\right]_{h=h_0}$$
$$= \frac{wc}{\delta}\left(\alpha_w + \frac{ch_0}{\delta}\right)\left(\frac{ch_0}{\delta}\right)^{-(\alpha_w+1)} e^{-ch_0/\delta}, \tag{A14}$$

$$w_2 = \frac{\partial^2}{\partial h^2}\left[-w\left(\frac{h}{\delta}\right)^{-\alpha_w} e^{-h/\delta}\right]_{h=h_0}$$
$$= -\frac{wc^2}{2\delta^2}\left[\left(\alpha_w + \frac{ch_0}{\delta}\right)^2 + \alpha_w\right]\left(\frac{ch_0}{\delta}\right)^{-(\alpha_w+2)} e^{-ch_0/\delta}, \tag{A15}$$

$$w_3 = \frac{\partial^3}{\partial h^3}\left[-w\left(\frac{h}{\delta}\right)^{-\alpha_w} e^{-h/\delta}\right]_{h=h_0}$$
$$= \frac{wc^2}{6\delta^2}\left[\left(\alpha_w + \frac{ch_0}{\delta}\right)^3 + \alpha_w\left(3\frac{ch_0}{\delta} + 3\alpha + 2\right)\right]$$
$$\times\left(\frac{ch_0}{\delta}\right)^{-(\alpha_w+3)} e^{-ch_0/\delta}. \tag{A16}$$

Equating terms with the same power of ε in the fully expanded Eq. (6), we get a set of linear differential equations. At the order of ε^1, we find that

$$L_0 h_1 + \tfrac{1}{4}(\partial_x^2 + \partial_y^2)h_1 = 0 \rightarrow (\partial_x^2 + \partial_y^2)\left(\partial_x^2 + \partial_y^2 + \tfrac{1}{2}\right)^2 h_1 = 0. \tag{A17}$$

The solutions to this equation are linear combinations of harmonic functions with a wave-number k_c. Note that the solution to $(\partial_x^2 + \partial_y^2)h_1 = 0$ is unbounded, and hence discarded. Square arrays, which are of primary interest to the authors, can be expanded as

$$h_1 = A_{11}e^{i\mathbf{k_1}\cdot\mathbf{x}} + A_{12}e^{i\mathbf{k}_2\cdot\mathbf{x}} + \text{c.c.}, \tag{A18}$$

where $\mathbf{k_1} = k_c(\cos\theta\hat{\mathbf{x}} + \sin\theta\mathbf{y})$ and $\mathbf{k}_2 = k_c(-\sin\theta\hat{\mathbf{x}} + \cos\theta\mathbf{y})$ are a pair of wave vectors perpendicular to each other and c.c. represents the complex conjugate.

At order ε^2, we find

$$L_0 h_2 + L_1 h_1 + \tfrac{1}{4}(\partial_x^2 + \partial_y^2)h_2 + \tfrac{1}{2}(\partial_X\partial_x + \partial_Y\partial_y)h_1 + w_2(\partial_x^2 + \partial_y^2)h_1^2 = 0. \tag{A19}$$

Using the expression (A18) we find

$$(\partial_x^2 + \partial_y^2)\left(\partial_x^2 + \partial_y^2 + \tfrac{1}{2}\right)^2 h_2 + w_2(\partial_x^2 + \partial_y^2)h_1^2 = 0. \tag{A20}$$

The solution to Eq. (A20) is found to be

$$h_2 = A_{21}e^{2i\mathbf{k_1}\cdot\mathbf{x}} + A_{22}e^{2i\mathbf{k}_2\cdot\mathbf{x}} + A_{23}e^{i(\mathbf{k_1}+\mathbf{k}_2)\cdot\mathbf{x}} + A_{24}e^{i(\mathbf{k_1}-\mathbf{k}_2)\cdot\mathbf{x}} + G + \text{c.c.}, \tag{A21}$$

where

$$A_{21} = -\tfrac{4}{9}w_2A_{11}^2,\quad A_{22} = -\tfrac{4}{9}w_2A_{12}^2,$$
$$A_{23} = -8w_2A_{11}A_{12},\quad \text{and}\quad A_{24} = -8w_2A_{11}\bar{A}_{12}. \tag{A22}$$

G is the Goldstone (zero wave vector) mode.[42] Since this mode is translational invariant, it usually decouples from other modes in the envelope equation.

At the order of ε^3, we have

$$\partial_T h_1 = L_0h_3 + L_2h_1 + L_1h_2 - (\partial_x^2 + \partial_y^2)[(\partial_x h_1)^2\partial_x^2 h_1] - q(\partial_x^2 + \partial_y^2)[(\partial_y h_1)^2\partial_x^2 h_1] - (\partial_x^2 + \partial_y^2)[(\partial_y h_1)^2\partial_y^2 h_1]$$
$$- q(\partial_x^2 + \partial_y^2)[(\partial_x h_1)^2\partial_y^2 h_1] - 4q(\partial_x^2 + \partial_y^2)[\partial_x h_1\partial_y h_1\partial_x\partial_y h_1] + \tfrac{1}{4}(\partial_x^2 + \partial_y^2)h_3 - r_2(\partial_x^2 + \partial_y^2)h_1 + 2w_2(\partial_x^2 + \partial_y^2)(h_1h_2)$$
$$+ w_3(\partial_x^2 + \partial_y^2)h_1^3 + \tfrac{1}{2}(\partial_X\partial_x + \partial_Y\partial_y)h_2 + 2w_2(\partial_X\partial_x + \partial_Y\partial_y)h_1^2 + \tfrac{1}{4}(\partial_X^2 + \partial_Y^2)h_1. \tag{A23}$$

The repeated application of Fredholm alternative on Eq. (A23) gives us

$$\frac{\partial A_{11}}{\partial T} = (\cos\theta\partial_X + \sin\theta\partial_Y)^2A_{11} - \frac{1}{8}|A_{11}|^2A_{11}(\cos^4\theta + 6q\cos^2\theta\sin^2\theta + \sin^4\theta) - \frac{1}{4}|A_{12}|^2A_{12}(q\cos^4\theta - 4q\cos^2\theta\sin^2\theta$$
$$+ 2\cos^2\theta\sin^2\theta + q\sin^4\theta) + \frac{1}{2}r_2A_{11} - w_2(\bar{A}_{11}A_{21} + A_{11}G + A_{12}A_{24} + \bar{A}_{12}A_{23}) - \frac{1}{2}w_3(3|A_{11}|^2A_{11} + 6|A_{12}|^2A_{11}), \tag{A24}$$

$$\frac{\partial A_{12}}{\partial T} = (-\sin\theta\partial_x + \cos\theta\partial_y)^2A_{12} - \frac{1}{8}|A_{12}|^2A_{12}(\cos^4\theta + 6q\cos^2\theta\sin^2\theta + \sin^4\theta) - \frac{1}{4}|A_{11}|^2A_{11}(q\cos^4\theta - 4q\cos^2\theta\sin^2\theta$$
$$+ 2\cos^2\theta\sin^2\theta + q\sin^4\theta) + \frac{1}{2}r_2A_{12} - w_2(\bar{A}_{12}A_{22} + A_{12}G + A_{11}A_{24} + \bar{A}_{11}A_{23}) - \frac{1}{2}w_3(3|A_{12}|^2A_{12} + 6|A_{11}|^2A_{12}). \tag{A25}$$

For the case $q=0$ (highly anisotropic surface energy), Eqs. (A24) and (A25) can be rescaled back to normal state variables. Defining $A_1=\varepsilon A_{11}$ and $B=\varepsilon G$, then we have

$$\frac{\partial A_1}{\partial t} = (\cos\theta\partial_x + \sin\theta\partial_y)^2 A_1 + g_1|A_1|^2A_1 + g_2|A_2|^2A_2 - w_2A_1B + \frac{1}{2}rA_1, \tag{A26}$$

$$\frac{\partial A_2}{\partial t} = (-\sin\theta\partial_x + \cos\theta\partial_y)^2 A_2 + g_1|A_2|^2A_2 + g_2|A_1|^2A_1 - w_2A_2B + \frac{1}{2}rA_2, \tag{A27}$$

where $g_1=\frac{4}{9}w_2^2-\frac{1}{8}(\cos^4\theta+\sin^4\theta)-\frac{3}{2}w_3$ and $g_2=16w_2^2-\frac{1}{2}\cos^2\theta\sin^2\theta-3w_3$.

The expansion has to be carried out at order ε^4 to derive the dynamics for the zero frequency mode,

$$\frac{\partial B}{\partial t} = \frac{1}{4}(\partial_x^2+\partial_y^2)B + 2w_2(\partial_x^2+\partial_y^2)(|A_1|^2+|A_2|^2). \tag{A28}$$

Equations (A26)–(A28) form the amplitude equations for square arrays, which consist of two stripe arrays normal to each other. The amplitude equation for striped arrays can be obtained by setting the amplitude of one of the arrays to zero, giving

$$\frac{\partial A}{\partial t} = (\cos\theta\partial_x + \sin\theta\partial_y)^2 A + g_1|A|^2A - w_2AB + \frac{1}{2}rA, \tag{A29}$$

$$\frac{\partial B}{\partial t} = \frac{1}{4}(\partial_x^2+\partial_y^2)B + 2w_2(\partial_x^2+\partial_y^2)|A|^2. \tag{A30}$$

The steady-state solution[43] to Eqs. (A26)–(A28) is the perfect square pattern $A_1=R_0e^{ikx}$, $A_2=R_0e^{iky}$ with $\theta=0$ and $B=0$, and

$$k^2 = g_1R_0^2 + g_2R_0^2 + \tfrac{1}{2}r.$$

In order to examine the stability of a square array, we perturb the system as

$$A_1 = R_0(1+a_1)e^{ikx+\phi}, \quad A_2 = R_0(1+a_2)e^{ikx+\varphi}, \quad B = b. \tag{A31}$$

Substituting Eq. (A31) into Eqs. (A26)–(A28), and separating the real and imaginary terms, we have

$$\partial_t a_1 = \partial_x^2 a_1 - 2k\partial_x\phi + 2g_1R_0^2a_2 - w_2b, \tag{A32}$$

$$\partial_t a_2 = \partial_y^2 a_2 - 2k\partial_y\phi + 2g_1R_0^2a_1 - w_2b, \tag{A33}$$

$$\partial_t b = \tfrac{1}{4}(\partial_x^2+\partial_y^2)b + 4R_0^2w_2(\partial_x^2+\partial_y^2)(a_1+a_2). \tag{A34}$$

The infinitesimal amplitude perturbation can be expressed in Fourier modes

$$a_1 = \hat{a}_1e^{\sigma t+imx+ily}, \quad a_2 = \hat{a}_2e^{\sigma t+imx+ily}, \quad b = \hat{b}e^{\sigma t+imx+ily}.$$

With fixed ϕ and φ, we may find out the growth rates corresponding to the amplitude modes $(\hat{a}_1+\hat{a}_2)$ and $(\hat{a}_1-\hat{a}_2)$ are

$$\sigma_1 = 2R_0^2(g_1-g_2), \tag{A35}$$

$$\sigma_2 = 2R_0^2(g_1+g_2). \tag{A36}$$

Square arrays are stable when $\sigma_1<0$ and $\sigma_2<0$. Similarly, the stability conditions for a striped array can be derived as

$$\sigma_1 = -\tfrac{5}{8}m^2 + g_1R_0^2 + \sqrt{-\tfrac{3}{4}m^2g_1R_0^2 + (g_1R_0^2)^2 + 4w_0^2m^2}, \tag{A37}$$

$$\sigma_2 = -\tfrac{5}{8}m^2 + g_1R_0^2 - \sqrt{-\tfrac{3}{4}m^2g_1R_0^2 + (g_1R_0^2)^2 + 4w_0^2m^2}. \tag{A38}$$

Note that Eqs. (A35) and (A36) and Eqs. (A37) and (A38) are the general stability conditions for square and striped patterns, respectively. Now, we are able to deduce the types of patterns that can arise for film growth on specific substrate, provided all the material properties are known.

[1] Y. Arakawa, IEEE J. Sel. Top. Quantum Electron. **8**, 823 (2002).
[2] S. Nakamura, S. Pearton, and S. Fasol, *The Blue Laser Diode: The Complete Story* (Springer-Verlag, Berlin, 2002).
[3] P. Bhattacharya, *Quantum Well and Quantum Dot Lasers: From Strained-Layer and Self-Organized Epitaxy to High-Performance Devices* (Kluwer, Dordrecht, 2000).
[4] D. G. Deppe and D. L. Huffaker, Appl. Phys. Lett. **77**, 3325 (2000).
[5] Y. Chye, M. E. White, E. Johnston-Halperin, B. D. Gerardot, D. D. Awschalom, and P. M. Petroff, Phys. Rev. B **66**, 201301 (2002).
[6] T. Lundstrom, W. Schoenfeld, H. Lee, and P. M. Petroff, Science **286**, 2312 (1999).
[7] P. M. Petroff, *Single Quantum Dots. Fundamentals, Applications, and New Concepts*, Topics in Applied Physics Vol. 90 (Springer-Verlag, Berlin, 2003), pp. 1–24.
[8] P. Alivisatos, Pure Appl. Chem. **72**, 3 (2000).
[9] P. Bhattacharya, A. D. Stiff-Roberts, S. Krishna, and S. Kennerly, Int. J. High Speed Electron. Syst. **12**, 969 (2002).
[10] S. Bandhyopadhyay and H. S. Nalwa, *Quantum Dots and Nano-Wires* (American Scientific, Stephenson Ranch, CA, 2003).
[11] D. Bimberg, Semiconductors **33**, 951 (1999).
[12] D. Bimberg, M. Grandmann, and N. N. Lendenstov, *Quantum Dot Heterostructures* (Wiley, New York, 1996).
[13] M. Grundmann, O. Stier, and D. Bimberg, Phys. Rev. B **52**, 11969 (1995).
[14] J. Tersoff, C. Teichert, and M. G. Lagally, Phys. Rev. Lett. **76**, 1675 (1996).
[15] M. H. Baier, S. Watanabe, E. Pelucchi, and E. Kapon, Appl. Phys. Lett. **84**, 1943 (2004).
[16] L. V. Asryan and S. Luryi, *Temperature-Insensitive Semiconductor Quantum Dot Laser* (Elsevier, New York, 2003).
[17] V. I. Belyavskii and S. V. Shevtsov, Semiconductors **36**, 821 (2002).
[18] R. Cingolani and R. Rinaldi, Phys. Status Solidi B **234**, 411 (2002).
[19] D. G. Deppe, S. Freisem, H. Huang, and S. Lipson, J. Phys. D **38**, 2119 (2005).
[20] O. Qasaimeh, IEEE Trans. Electron Devices **50**, 1575 (2003).
[21] V. A. Shchukin and D. Bimberg, Rev. Mod. Phys. **71**, 1125 (1999).
[22] A. A. Golovin, M. S. Levine, T. V. Savina, and S. H. Davis, Phys. Rev. B **70**, 235342 (2004).
[23] S. Christiansen, M. Albrecht, H. P. Strunk, P. O. Hansson, and E. Bauser, Appl. Phys. Lett. **66**, 574 (1995).
[24] I. Daruka and A.-L. Barabasi, Phys. Rev. Lett. **79**, 3708 (1997).
[25] Y. Pang and R. Huang, Phys. Rev. B **74**, 075413 (2006).
[26] K. Kern, H. Niehus, A. Schatz, P. Zeppenfeld, J. Goerge, and G. Comsa, Phys. Rev. Lett. **67**, 855 (1991).

[27]K. Pohl, M. C. Bartelt, J. de la Figuera, N. C. Bartelt, J. Hrbek, and R. Q. Hwang, Nature (London) **397**, 238 (1999).
[28]R. Plass, J. A. Last, N. C. Bartelt, and G. L. Kellogg, Nature (London) **412**, 875 (2001).
[29]Q. Wei, J. Lian, W. Li, and L. Wang, Phys. Rev. Lett. **100**, 076103 (2008).
[30]Z. Suo and W. Hong, Proc. Natl. Acad. Sci. U.S.A. **101**, 7874 (2004).
[31]Y. F. Gao and Z. Suo, J. Appl. Phys. **93**, 4276 (2003).
[32]J. Y. Cheng, C. A. Ross, H. I. Smith, and E. L. Thomas, Adv. Mater. (Weinheim, Ger.) **18**, 2505 (2006).
[33]R. V. Kukta and D. Kouris, J. Appl. Phys. **97**, 033527 (2005).
[34]F. Shi, P. Sharma, D. J. Kouri, F. Hussain, and G. H. Gunaratne, Phys. Rev. E **78**, 025203 (2008).
[35]R. J. Asaro and W. A. Tiller, Metall. Mater. Trans. B **3**, 1789 (1972).
[36]M. A. Grinfel'd, Sov. Phys. Dokl. **31**, 831 (1986).
[37]W. W. Mullins, J. Appl. Phys. **28**, 333 (1957).
[38]A. C. Newell and J. A. Whitehead, J. Fluid Mech. **38**, 279 (1969).
[39]L. A. Segel, J. Fluid Mech. **38**, 203 (1969).
[40]*Handbook of Nanotechnology*, edited by B. Bushan (Springer, New York, 2003).
[41]G. H. Gunaratne, O. Qi, and H. L. Swinney, Phys. Rev. E **50**, 2802 (1994).
[42]P. C. Matthews and S. M. Cox, Nonlinearity **13**, 1293 (2000).
[43]R. B. Hoyle, in *Time-Dependent Non-Linear Convection*, edited by P. A. Tyvand (Computational Mechanics, Southampton, 1998).